THE JOURNAL OF NAVIGATION (2020), **73**, 746–762.
doi:10.1017/S0373463319000973

Real-Time Estimation and Calibration of GLONASS Inter-Frequency Phase and Code Bias

Zhixin Yang, Hui Liu, Yidong Lou, Bao Shu, Longwei Xu, Yifei Wang and Baofei Xie

(*GNSS Research Center, Wuhan University, Wuhan, China*)
(E-mail: ydlou@whu.edu.cn)

The frequency division multiple access (FDMA) strategy used in GLONASS causes inter-frequency phase bias (IFPB) and inter-frequency code bias (IFCB) between receivers from different manufacturers. The existence of IFPB and IFCB significantly increases the difficulties of fixing GLONASS ambiguity and limits the accuracy and reliability of GLONASS positioning. Moreover, the initial value of IFPB and IFCB may be unavailable or unreliable with the increasing number of receivers from different manufacturers in recent years. In this study, a real-time and reliable calibration algorithm of IFPB and IFCB based on multi-GNSS assistance is proposed by providing a fixed solution. Real-time IFPB rate and IFCB can be obtained using this algorithm without the initial IFPB and IFCB. The IFPB rate for all GLONASS satellites and IFCB for each GLONASS satellite are estimated due to different characteristics of IFPB and IFCB. IFPB calibration can be divided into constant and real-time IFPB calibrations to meet the different positioning requirements. Results show that constant IFPB rate has only 2 mm difference from the mean value of real-time IFPB rate. The IFPB rate and IFCB estimated by this algorithm have excellent stability, and the change in reference satellite cannot affect the results of IFPB rate and the stability of IFCB. The centimetre-level positioning results can be obtained using two calibration methods, and the positioning results with real-time calibration method are 10%–20% better than those with the constant calibration method. Under satellite-deprived environments, the improvements of multi-GNSS positioning accuracy with constant inter-frequency bias calibration gradually increase as the satellite cut-off elevation angle increases compared with GPS/BDS, which can reach up to 0·9 cm in the vertical direction.

KEYWORDS

1. GLONASS. 2. Multi-GNSS. 3. Inter-Frequency Phase Bias (IFPB). 4. Inter-Frequency Code Bias (IFCB).

Submitted: 26 February 2019. Accepted: 11 November 2019. First published online: 26 December 2019.

1. INTRODUCTION. Multi-GNSS navigation and positioning is an inevitable trend caused by the modernisation programme of GPS and GLONASS and the rapid development of the BDS and Galileo programmes. The participation of the GLONASS system can increase the number of visible satellites as appropriate and improve the positioning performance of GNSS. Unlike GPS/BDS/Galileo, GLONASS employs a frequency division

multiple access (FDMA) strategy and transmits signals on 14 frequencies (frequency number from −7 to 6). Given the difference in signal wavelength between GLONASS satellites, however, receiver hardware delay cannot be eliminated in double-difference (DD) observation for an inhomogeneous baseline that consists of receivers from different manufacturers, thereby bringing in inter-frequency bias (IFB) issues in GLONASS phase and pseudorange observations (Wanninger and Wallstab-Freitag, 2007; Takac, 2009; Yamada et al., 2010; Reussner and Wanninger, 2011; Wanninger, 2012). The existence of IFPB and IFCB significantly increases the difficulties of fixing GLONASS ambiguity and limits the accuracy and reliability of GLONASS positioning (Shi et al., 2013; Yao et al., 2017; Tian et al., 2018).

The Russian Federation has planned to add code division multiple access (CDMA) signal to the GLONASS signal structure as part of its modernisation programme since 2008 (Revnivykh, 2011). However, Russian Space Agency officials have indicated that FDMA signals will be retained in Glonass-K2 and Glonass-KM satellites in the future to ensure the compatibility of FDMA receivers. Therefore, the issues of GLONASS IFPB and IFCB will continue in the next few years (Takac, 2009; Karutin and Inst, 2015).

There have been many attempts by researchers to investigate the characteristics of GLONASS IFPB and IFCB and to calibrate these biases. Pratt et al. (1998) suggested that GLONASS IFPB has a linear relationship with the frequency number. Wanninger and Wallstab-Freitag (2007) confirmed this finding in several baselines of various GPS/GLONASS receivers, which can be utilised to model IFPB, so that they can be estimated by one IFPB rate parameter. Reussner and Wanninger (2011) verified that IFCB is mainly a frequency function, but simple linear modelling is insufficient, which even show large difference between receivers from the same manufacturer. Wanninger (2012) employed single-difference (SD) GPS and GLONASS observations to determine the GLONASS IFPB rates and proved that the IFPB rates are similar for L1 and L2 and also for receivers of the same type. However, this method requires knowing the initial value of the IFPB rate with a certain accuracy so that at least one ambiguity needs to be fixed. Al-Shaery et al. (2013) estimated the IFPB and IFCB rates with float ambiguity parameters and discovered that IFCB can reach up to several metres. However, the IFPB and IFCB rates used in the experiment were estimated from a zero baseline in advance, which cannot meet the needs of fast and real-time estimation of IFPB rates. Banville et al. (2013) also proposed a new approach without any external initial value to calibrate IFPB rate by observing two GLONASS satellites with adjacent frequency numbers simultaneously. Shi et al. (2013) demonstrated that the IFCB of two receivers with the same firmware may be different because of various antenna types, and their differences are closely related to frequency, which should be provided for each satellite because IFCB may vary even on the same frequency. Tian et al. (2015) and Tian et al. (2018) presented a method for the real-time estimated IFB rate based on particle filter without an initial value. However, the performance of this algorithm is exhaustive, and the computational efficiency is unsatisfactory. Yao et al. (2017) proposed an estimation method of IFPB rate with single-epoch or Kalman filter algorithm, but the accuracy of the initial IFPB rate is low due to the discrepancy of the IFPB rate between L1 and L2 bands and the existence of IFCB.

Although the IFPB and IFCB problems in GLONASS have been researched thoroughly, the methods proposed to solve them still cannot meet the needs of fast real-time positioning.

https://doi.org/10.1017/S0373463319000973 Published online by Cambridge University Press

On the one hand, initial IFPB and IFCB should be provided when GLONASS satellites participate in multi-GNSS positioning, whereas the initial IFPB and IFCB may be unavailable or unreliable due to the increasing number of receivers produced by different manufacturers in recent years (Jiang et al., 2017; Yao et al., 2017; Tian et al., 2018). On the other hand, IFPB and IFCB are susceptible to different receiver firmware versions, antenna types and other factors (Wanninger and Wallstab-Freitag, 2007; Shi et al., 2013), which cause inconsistencies in the initial IFPB and IFCB with the actual bias.

In this study, a fast, real-time, accurate and reliable estimation and calibration algorithm for IFPB and IFCB is proposed on the basis of multi-GNSS assistance, such as GPS and BDS. In this algorithm, real-time IFPB rate and IFCB can be obtained without the initial IFPB and IFCB based on multi-GNSS assistance, which provides fixed solution coordinates. IFPB calibration can be divided into constant and real-time IFPB calibration to meet the different positioning requirements. This algorithm can solve the issues of no initial IFPB and IFCB or inaccurate initial value and further improve the combined positioning performance between GLONASS and other multi-GNSS, especially under GNSS satellite-deprived environments.

2. REAL-TIME ESTIMATION AND CALIBRATION ALGORITHM OF IFPB AND IFCB.

2.1. *Mathematical modelling.* In the process of multi-GNSS real-time kinematic (RTK) positioning, satellite orbit bias, satellite and receiver clock bias, ionospheric delay and tropospheric delay have spatial correlation between base and rover stations, especially in short or medium baselines. Therefore, most of these correlation biases can be eliminated or weakened by the DD observation model in relative positioning.

For GPS or BDS, given the adoption of CDMA technology, all signals transmitted by satellites have the same wavelength on each frequency band, which are processed through a series of identical components at the RF front-end. The hardware delay of the phase and pseudorange observations only contains the same constant part, which can be eliminated by DD processing. Therefore, IFPB and IFCB do not occur in GPS/BDS observations. The GPS/BDS DD pseudorange and phase observation equation can be described as follows:

$$\begin{cases} \rho_{rb,f}^{ij,G/C} = r_{rb,f}^{ij,G/C} + I_{rb,f}^{ij,G/C} + T_{rb,f}^{ij,G/C} + \varepsilon_{\rho,rb}^{ij,G/C} \\ \lambda \cdot \varphi_{rb,f}^{ij,G/C} = r_{rb,f}^{ij,G/C} - \lambda \cdot N_{rb,f}^{ij,G/C} - I_{rb,f}^{ij,G/C} + T_{rb,f}^{ij,G/C} + \varepsilon_{\varphi,rb}^{ij,G/C} \end{cases} \tag{1}$$

where superscripts i and j refer to satellites; superscript G/C indicates the GPS or BDS system; subscripts b and r stand for base and rover stations, respectively; subscript f refers to the signal frequency; $\rho_{rb,f}^{ij,G/C}$ and $\varphi_{rb,f}^{ij,G/C}$ refer to DD pseudorange and phase observation of GPS/BDS on frequency f, respectively; $r_{rb,f}^{ij,G/C}$ is the DD range between satellite and receiver; $I_{rb,f}^{ij,G/C}$ and $T_{rb,f}^{ij,G/C}$ represent DD ionospheric and tropospheric delay, respectively; λ is the signal wavelength; $N_{rb,f}^{ij,G/C}$ represents DD phase ambiguity; $\varepsilon_{\rho,rb}^{ij,G/C}$ and $\varepsilon_{\varphi,rb}^{ij,G/C}$ represent the sum of all uncorrected systematic and random errors in the DD pseudorange and phase observation, respectively. In addition, satellite orbit bias and multipath errors are not represented in Equation (1).

https://doi.org/10.1017/S0373463319000973 Published online by Cambridge University Press

Unlike GPS or BDS, the GLONASS system employs FDMA technology, which causes all signals transmitted by GLONASS satellites to have different wavelengths on each frequency band, and different satellites are identified by various frequencies. Therefore, the hardware delay of GLONASS observations varies with signals' frequencies, and these hardware delays consist of a constant part and a frequency-dependent part (Wanninger, 2012). The constant part can be absorbed by the receiver clock bias similar to GPS and BDS, and the residuary hardware delay of the frequency-dependent part causes IFPB and IFCB after DD processing.

IFPB is primarily related to receiver manufacturer and has a linear relationship with signal frequency. The SD and DD IFPB can be expressed as follows:

$$\begin{cases} b_{b,f}^{i,R} - b_{b,f}^{j,R} = (b_{b,f}^{R} + k^i \cdot \delta b_{b,f}^{R}) - (b_{b,1}^{R} + k^j \cdot \delta b_{b,f}^{R}) = (k^i - k^j) \cdot \delta b_{b,f}^{R} \\ (b_{r,f}^{i,R} - b_{r,f}^{j,R}) - (b_{b,f}^{i,R} - b_{b,f}^{j,R}) = (k^i - k^j) \cdot (\delta b_{r,f}^{R} - \delta b_{b,f}^{R}) = k^{ij} \cdot \delta b_{rb,f}^{R} \end{cases} \tag{2}$$

where superscript R indicates the GLONASS system; $b_{b,f}^{i,R}$ refers to the hardware delay of the phase observation of satellite i received by the receiver of station b on frequency f; $b_{b,f}^{R}$ represents the constant part of the hardware delay; k is the GLONASS frequency number; $k^i \cdot \delta b_{b,f}^{R}$ represents the frequency-dependent part of the hardware delay; $k^{ij} \cdot \delta b_{rb,f}^{R}$ stands for IFPB after DD process; and $\delta b_{rb,f}^{R}$ is mainly related to receiver manufacturer, which is usually called the IFPB rate between stations r and b on frequency f.

Calibrating the effects of IFCB is difficult, however, due to the complicated characteristics of IFCB compared with IFPB. No obvious linear relationship can be observed between IFCB and GLONASS frequency numbers, and IFCB is extremely susceptible to receiver firmware version, antenna type and other factors. In addition, IFCB still occurs even with a homogeneous baseline that consists of receivers from the same manufacturer. Therefore, the IFCB should be estimated on each satellite (Shi et al., 2013; Song et al., 2014; Liu et al., 2016). Considering IFPB and IFCB, GLONASS DD phase and pseudorange observation equations can be described as

$$\begin{cases} \rho_{rb,f}^{ij,R} = r_{rb,f}^{ij,R} + B_{rb,f}^{i} - B_{rb,f}^{j} + I_{rb,f}^{ij,R} + T_{rb,f}^{ij,R} + \varepsilon_{\rho,rb}^{ij,R} \\ \Phi_{rb,f}^{ij,R} = r_{rb,f}^{ij,R} - (\lambda_i^R - \lambda_j^R) \cdot N_{rb,f}^{j,R} - \lambda_i^R \cdot N_{rb,f}^{ij,R} + k^{ij} \cdot \delta b_{rb,f} - I_{rb,f}^{ij,R} + T_{rb,f}^{ij,R} + \varepsilon_{\varphi,rb}^{ij,R} \end{cases} \tag{3}$$

where $\Phi_{rb,f}^{ij,R} = \lambda_i \cdot \varphi_{rb,f}^{i,R} - \lambda_j \cdot \varphi_{rb,f}^{j,R}$ represents GLONASS phase observation after DD processing, $(\lambda_i^R - \lambda_j^R) \cdot N_{rb,f}^{j,R} - \lambda_i^R \cdot N_{rb,f}^{ij,R}$ is the transformation form of GLONASS DD ambiguity to obtain integer characteristics of GLONASS ambiguity (Wang, 2000; Takac, 2009), $N_{rb,f}^{j,R}$ refers to SD ambiguity of GLONASS reference satellite, and $B_{rb,f}^{i}$ is the IFCB of satellite i between stations b and r. Other variables have the meanings stated previously.

During the process of calculating GLONASS measurements, the DD ionospheric delay will be eliminated by Klobuchar model correction instead of estimation. The DD zenith tropospheric dry delay will be eliminated by Saastamoinen model correction and DD zenith tropospheric wet delay will be provided by the estimation results of GPS/BDS. From Equation (3), the IFPB rate and IFCB, station coordinates and DD ambiguity need to be estimated. The station coordinates and IFCB do not need to be estimated simultaneously in GLONASS pseudorange observation equations due to multi-GNSS assistance and IFCB calibration.

https://doi.org/10.1017/S0373463319000973 Published online by Cambridge University Press

Different estimations and calibration strategies need to be implemented due to various statistical characteristics (Yamada et al., 2010; Reussner and Wanninger, 2011). In this study, the IFPB rates for all GLONASS satellites and the IFCB for each GLONASS satellite are estimated and calibrated.

2.2. *IFPB estimation and calibration.* In the algorithm of GLONASS IFPB estimation based on multi-GNSS assistance, the fixed solution of the GPS/BDS system will be calculated initially as rover approximate coordinates, and the parameters of float ambiguity and IFPB rate estimated using GLONASS DD observation by Kalman filter. The IFPB rates on L1 and L2 frequencies are estimated as different parameters, and the calculation model is shown as Equation (4). The constant IFPB rate will be obtained when GLONASS DD ambiguity can be accurately fixed by the LAMBDA algorithm. The initialisation verification will be completed if the ambiguity is successfully fixed for more than 10 epochs and the differences of IFPB estimation value between two epoch are less than 2 mm. After verifying the correctness and stability of the constant IFPB rate, the initialisation process of estimation IFPB is accomplished.

$$\Phi_{rb,f}^{ij,R} = k^{ij} \cdot \delta b_{rb,f}^{R} - (\lambda_i^R - \lambda_j^R) \cdot N_{rb,f}^{j,R} - \lambda_i^R \cdot N_{rb,f}^{ij,R} + l_{rb,f}^{ij,R} \tag{4}$$

where $l_{rb,f}^{ij,R} = (r_{r,f}^{i,R})_0^{G/C} - r_{b,f}^{i,R} - (r_{r,f}^{j,R})_0^{G/C} + r_{b,f}^{j,R} - I_{rb,f}^{ij,R} + T_{rb,f}^{ij,R}$ represents the constant portion after subtracting the known geometric distance and atmospheric delay.

After accomplishing the IFPB initialisation process, the constant IFPB calibration and real-time calibration method can be selected. In the method of constant IFPB calibration, given that most of the effects caused by IFPB can be eliminated by constant IFPB rate, GLONASS phase observations can be directly corrected with constant IFPB rate as a constant in Equation (3) and participate in the Kalman filter together with Equation (1) to obtain a highly accurate fixed solution of multi-GNSS. In the method of real-time IFPB calibration, the parameters of the IFPB rate can be estimated by Kalman filter together with coordinate components and ambiguity to obtain accurate fixed solutions and real-time IFPB rate due to the existence of the constant IFPB rate.

The flow chart of IFPB estimation and calibration is shown in Figure 1. If initialisation is not completed, only GPS/BDS positioning results are output, which are used as rover approximate coordinates to rapidly estimate the constant IFPB rate. Multi-GNSS positioning results will not be output until the IFPB initialisation process is correctly verified. Then constant IFPB calibration and real-time IFPB calibration method can be selected conveniently to meet the different requirements.

2.3. *IFCB estimation and calibration.* Similar to the IFPB estimation method, IFCB estimation is also based on multi-GNSS assistance, and the fixed solution of GPS/BDS is used as rover approximate coordinates, which are no longer estimated in the process of estimating IFCB. The IFCB of each satellite at each frequency needs to be estimated, however, because the IFCB for different satellites cannot be represented by a linear model (Shi et al., 2013; Liu et al., 2018). The IFCB estimation model on the frequency f is expressed as follows:

$$\rho_{rb,f}^{ij,R} = \delta B_{rb,f}^{ij} + l_{rb,f}^{ij,R} \tag{5}$$

where $\delta B_{rb,f}^{ij}$ represents the IFCB difference between satellites i and j and stations b and r on frequency f, which will be replaced by IFCB in this study and can be represented by Equation (6). The meaning of the constant term $l_{rb,f}^{ij,R}$ is the same as in Equation (5).

https://doi.org/10.1017/S0373463319000973 Published online by Cambridge University Press

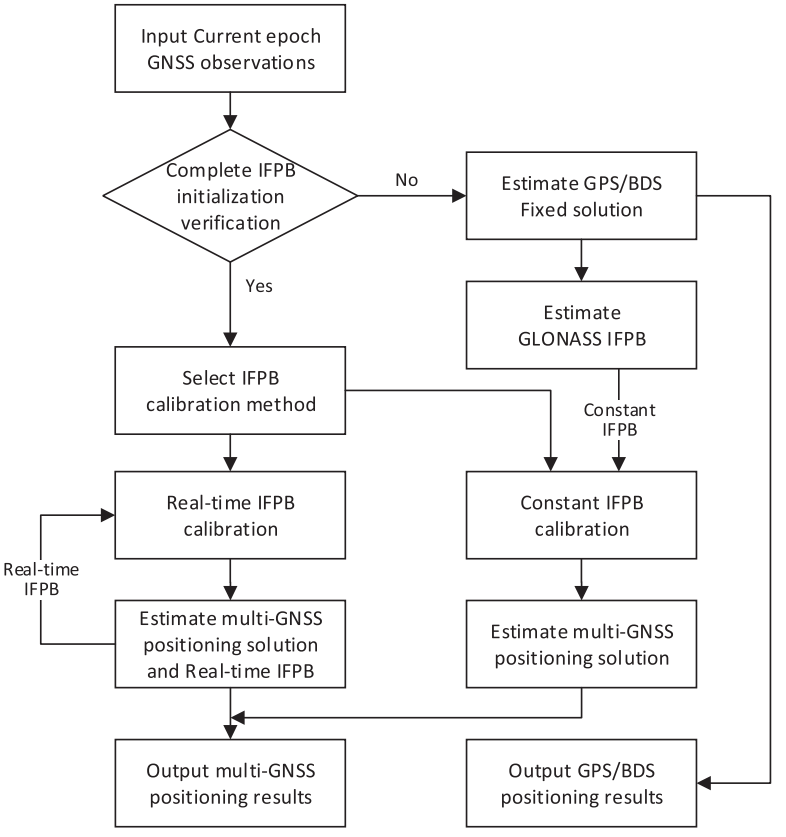

Figure 1. Flow chart of IFPB estimation and calibration.

The initialisation verification will be completed if the ambiguity is successfully fixed for more than 10 epochs and the differences of IFCB estimation value between two epochs are less than 10 cm.

$$\delta B^{ij}_{rb,f} = B^{i}_{rb,f} - B^{j}_{rb,f} \tag{6}$$

The IFCB cannot be calibrated directly as a constant similar to a constant IFPB rate because satellite lifting or changes in reference satellites is often encountered during positioning. Figure 2 shows the flow chart of IFCB estimation and calibration. The IFCB estimation process is performed based on the fixed solution provided by GPS and BDS to rapidly obtain the current epoch IFCB, which will not used for the next epoch GLONASS measurements calibration until the IFPB initialisation process is correctly verified. The next epoch IFCB continues to be updated, and the entire cycle process of IFCB estimation and calibration is implemented.

3. EXPERIMENT AND ANALYSIS OF RESULTS. In the experiment analysis section, the observation data include four types of baselines: zero, ultra-short, short and medium baseline. Each type of baseline contains inhomogeneous and homogeneous baselines for comparison. The observation data of the zero baselines were obtained

https://doi.org/10.1017/S0373463319000973 Published online by Cambridge University Press

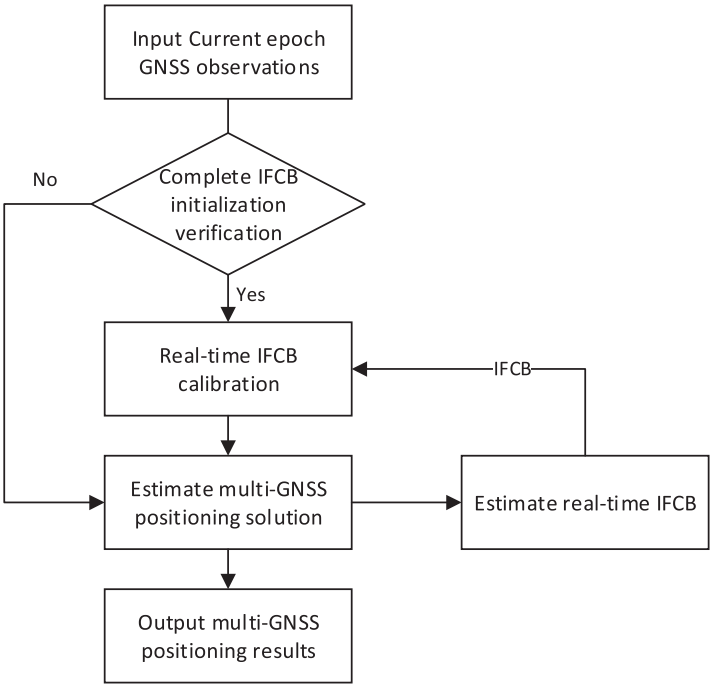

Figure 2. Flow chart of IFCB estimation and calibration.

Table 1. Baseline information of experiments.

Baseline type	Baseline name	Base receiver type	Rover receiver type	Baseline length	Date
Zero baseline	CUT0-CUT1	TRIMBLE NETR9	SEPT POLARX4	0·0 m	1 Oct. 2018
	CUT0-CUT2	TRIMBLE NETR9	TRIMBLE NETR9	0·0 m	1 Oct. 2018
Ultra-short baseline	WUS1-WUU1	COMNAV M300	STONEX S9	8·5 m	3 Mar. 2017
	WUS1-WUS2	COMNAV M300	COMNAV M300	8·3 m	3 Mar. 2017
Short baseline	HKWS-HKKS	LEICA GR25	TRIMBLE NETR9	7·7 km	1 Apr. 2017
	HKWS-HKSS	LEICA GR25	LEICA GR50	6·8 km	1 Apr. 2017
Medium baseline	HKKT-HKKS	LEICA GR50	TRIMBLE NETR9	26·7 km	1 Apr. 2017
	HKKT-HKWS	LEICA GR50	LEICA GR25	27·7 km	1 Apr. 2017

from Curtin GNSS Research Centre, Australia (http://saegnss2.curtin.edu.au/ldc/rawdata). The observation data of the ultra-short baselines were obtained from static collection at Wuhan University, China. The observation data of the short and medium baselines were obtained from the Hong Kong Satellite Positioning Reference Station Network (https://www.geodetic.gov.hk/sc/satref/downv.aspx). Table 1 shows the detailed information of all baselines in the experiment, including baseline type and name, base and rover receiver type and baseline length.

On the basis of the algorithm presented in Section 2, we analyse the experiment results to verify this algorithm in two parts. In the first part, the IFPB and IFCB estimation algorithms will be verified through the stable and reliable results of IFPB and IFCB rates. In the

https://doi.org/10.1017/S0373463319000973 Published online by Cambridge University Press

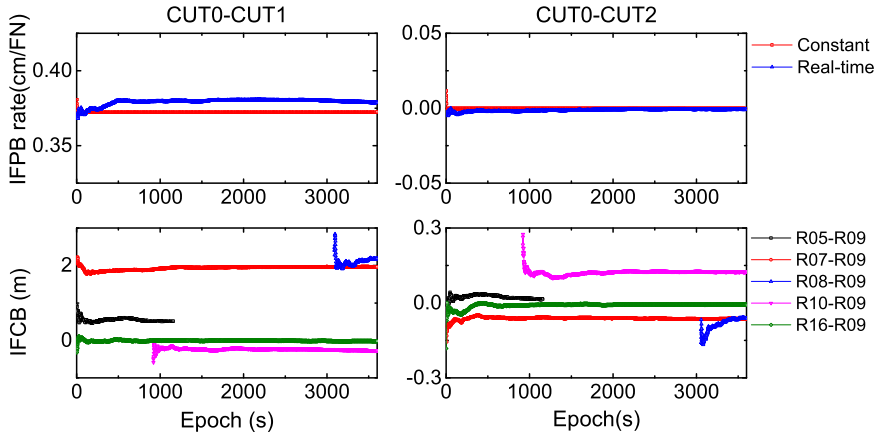

Figure 3. IFPB rate and IFCB for zero baselines (CUT0-CUT1 and CUT0-CUT2).

second part, two calibration methods, real-time and constant IFPB and IFCB calibration, will be verified through multiple baseline data. The enhancements of calibrated GLONASS observations for GPS/BDS positioning performance will be verified with different satellite cut-off elevation angles to simulate satellite-deprived environments. During the process of IFB estimation and positioning solution, the sampling interval is 1 s, and the satellite cut-off elevation angle is 15°, except for the experiments conducted in satellite-deprived environments.

Several terms used in the following sections are defined here, in advance. In this study, 'stability' has different meanings for IFPB rate and IFCB, respectively. If the standard deviation (STD) of real-time IFPB rates estimated in this algorithm were less than 0·3 mm, then we consider that the IFPB results are stable. Analogously, if the STD of real-time IFCBs estimated in this algorithm were less than 3 cm, then we consider that the IFCB results are stable. GLONASS normal positioning means that GLONASS satellites have sufficient numbers, at least two satellites, to participate in multi-GNSS RTK positioning and their ambiguity can be fixed correctly.

3.1. *Analysis of IFB estimation results.* We calculate the GLONASS IFPB rate for all GLONASS satellites and IFCB for each GLONASS satellite of the four types of baselines on L1 frequency to analyse the stability of IFPB and IFCB rates estimated by the algorithm presented in Section 2. The differences between the constant IFPB rates and the mean values of real-time IFPB rates and the STD of IFPB rate and IFCB are analysed. The situations of reference satellite change are also considered in these experiments.

The constant IFPB rate, real-time IFPB rate and IFCB of the four types of baselines are estimated, and each type of baseline contains inhomogeneous and homogeneous baselines. The sequence diagrams of the IFPB rate and IFCB of four types of baselines are shown in Figures 3–6. In each diagram in Figures 3–6, the two top subgraphs represent the IFPB rate, and red and blue represent the constant IFPB and IFPB rate, respectively. The two bottom subgraphs represent the IFCB between satellites and their reference satellite. The left and right subgraphs represent the inhomogeneous and homogeneous baselines, respectively. In Figure 6, the IFPB initialisation process was restarted after the failure of ambiguity resolution in the medium baseline HKKT-HKKS.

https://doi.org/10.1017/S0373463319000973 Published online by Cambridge University Press

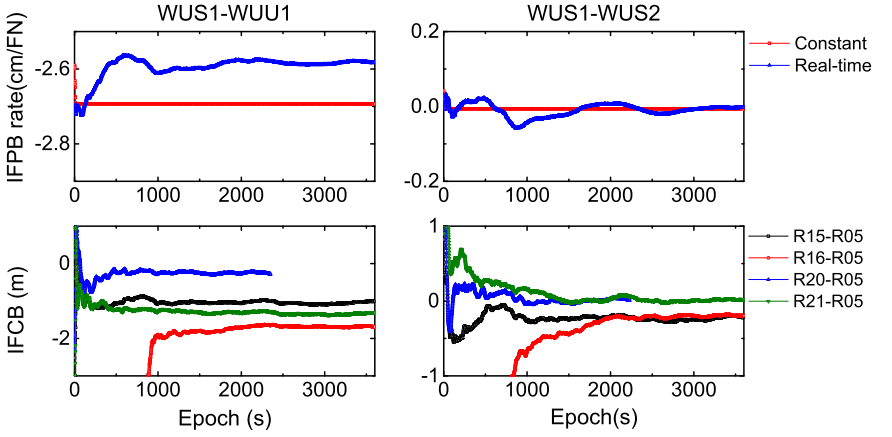

Figure 4. IFPB rate and IFCB for ultra-short baselines (WUS1-WUU1 and WUS1-WUS2).

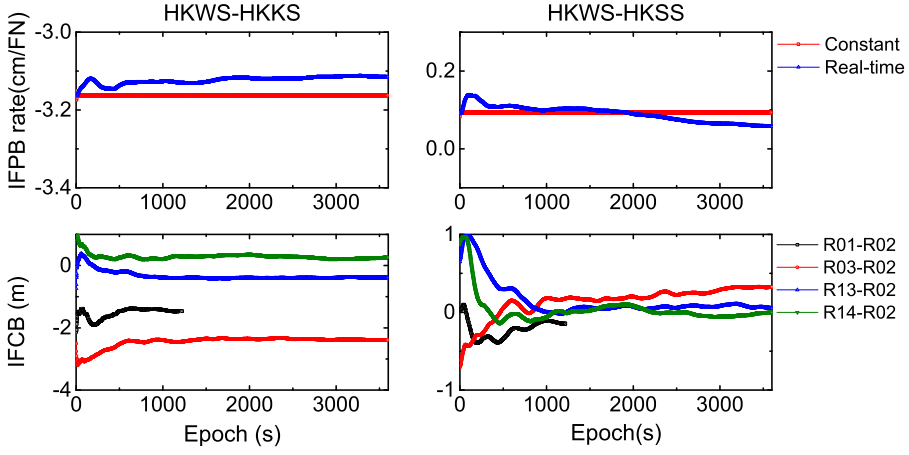

Figure 5. IFPB rate and IFCB for short baselines (HKWS-HKKS and HKWS-HKSS).

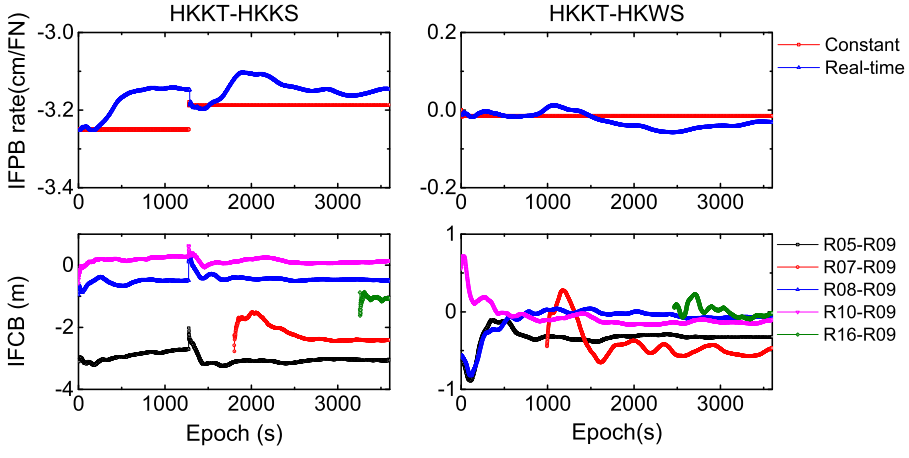

Figure 6. IFPB rate and IFCB for medium baselines (HKKT-HKKKS and HKKT-HKWS).

https://doi.org/10.1017/S0373463319000973 Published online by Cambridge University Press

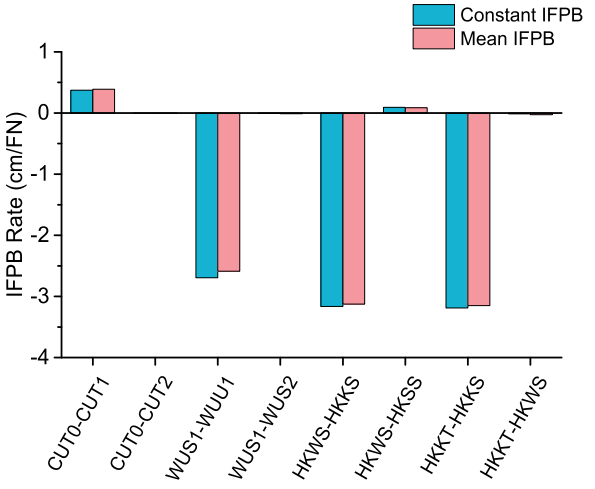

Figure 7. IFPB rates for the four types of baselines (zero, ultra-short, short and medium baselines).

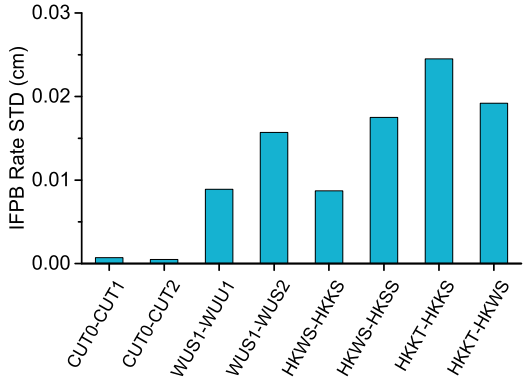

Figure 8. IFPB rate STD for all types of baselines (zero, ultra-short, short and medium baselines).

In the two top subgraphs from Figures 3–6, whether the baseline is short or medium, the estimated real-time IFPB rates are so stable that their change range is less than 3 mm. The differences between constant and real-time IFPB rates are also within 3 mm. Figure 7 shows the statistical results of constant IFPB rate and the mean value of real-time IFPB rate of the four types of inhomogeneous and homogeneous baselines. In Figure 7, the differences between the constant IFPB rates and the mean value of real-time IFPB rates are extremely small, both being less than 2 mm. The IFPB rates of the inhomogeneous baselines are generally at the centimetre level. By contrast, the IFPB rates of the homogeneous baselines are generally less than 1 mm, indicating that their IFPB has been eliminated during the DD process. Figure 8 shows the STD statistics for real-time IFPB rates estimated from all baselines, which are less than 0·3 mm. Moreover, the stability of IFPB rates will be improved when the baseline is shortened.

The initialisation process is implemented every 3 min to analyse the IFPB initialisation time of IFPB estimation. Table 2 shows the average times of 20 initialisation processes for

https://doi.org/10.1017/S0373463319000973 Published online by Cambridge University Press

Table 2. Average initialisation time of IFPB estimation for four types of baselines.

Initialisation time (s)	Zero baseline	Ultra-short baseline	Short baseline	Medium baseline
Inhomogeneity	11·2	11·3	36·1	147·6
Homogeneity	11·1	11·4	32·9	97·5

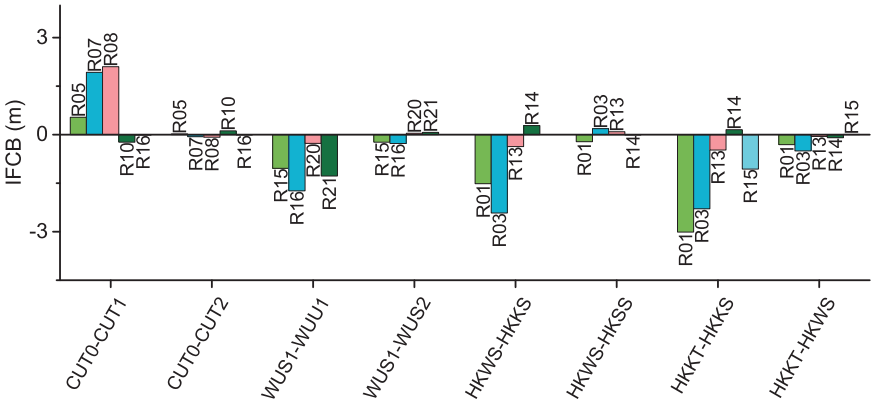

Figure 9. IFCB for four types of baselines.

all types of baselines for 1 h. Table 2 shows that the initialisation process of IFPB estimation can be implemented within several seconds for short baseline and several minutes for medium baseline.

The two subgraphs from Figures 3–6 show that the IFCB between inhomogeneous baselines can converge to a stable value within 200–400 epochs. Figure 9 shows the statistical results for the IFCBs of four types of inhomogeneous and homogeneous baselines. The IFCBs of inhomogeneous baselines can be as high as several metres, whereas the IFCBs of homogeneous baselines are generally within 5 cm. Figure 10 shows the variance statistics for real-time IFCB estimated from all baselines. The variances in IFCB are within 0·2 m for all homogeneous baselines. Similar to the IFPB rate, IFCB also shows remarkable stability with short baselines. Moreover, even for medium baselines, the STD of IFCB between homogeneous baselines remains small.

The IFCB of all satellites will change with the switch of the reference satellite. Therefore, to analyse the stability of the IFCB, 1 h observation data with no change in the reference satellite was used in this study. Figure 11 shows the estimation of the IFPB rate and IFCB for baseline CUT0-CUT1 with 3 h observation data. In Figure 11, when the reference satellite changes, IFPB rate varies slightly and IFCB remains stable after the conversion of reference satellite IFCB.

3.2. *Positioning performance analysis.* After the estimation of stable results for the IFPB rate and IFCB in previous sections, we will analyse the positioning performance in this section. First, the positioning results with IFB calibration will be compared with no IFB calibration and with GPS/BDS to verify the necessity of IFB calibration. The influence of IFPB accuracy on positioning results and fixed rates is analysed to verify the availability of constant and real-time IFPB rates estimated by this algorithm. The positioning results

https://doi.org/10.1017/S0373463319000973 Published online by Cambridge University Press

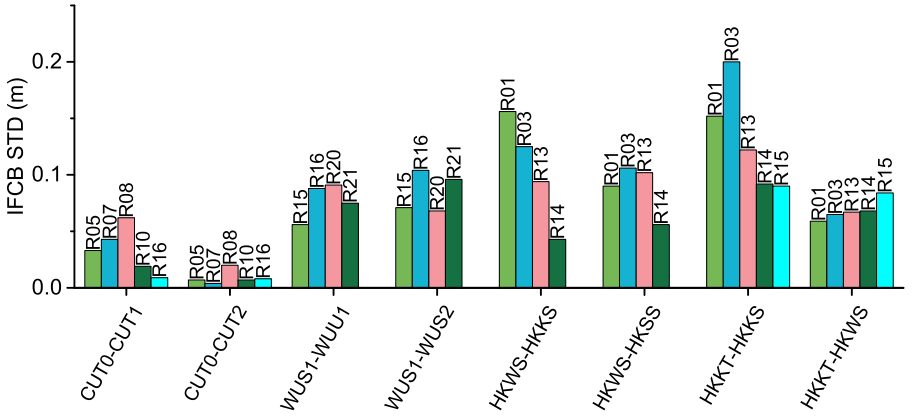

Figure 10. IFCB STD for four types of baselines.

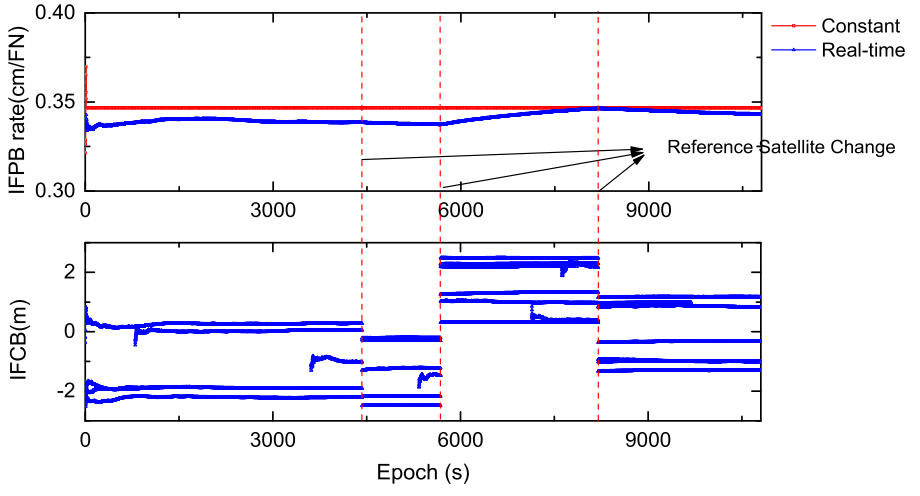

Figure 11. IFPB rate and IFCB for baseline CUT0-CUT1 with 3 h observations.

and fixed rates with two calibration methods (real-time and constant IFPB and IFCB calibration) are then analysed and contrasted with GPS/BDS. Finally, the enhancements of calibrated GLONASS observations for GPS/BDS positioning performance will be verified with different satellite cut-off elevation angles to simulate satellite-deprived environments.

The multi-GNSS positioning results calculated with IFB calibration will be compared with no IFB calibration to verify the necessity of IFB calibration in this algorithm. Moreover, we also calculate the positioning results of GPS/BDS to reflect the significance of GLONASS measurements separately. Figure 12 shows the GNSS position errors of two inhomogeneous baselines with IFB calibration compared with no IFB calibration and GPS/BDS. The three subgraphs indicate the positioning results of baseline CUT0-CUT1, and the three subgraphs indicate the positioning results of baseline HKWS-HKKS. In Figure 12, without IFB calibration, the zero-baseline GLONASS ambiguity can be fixed

https://doi.org/10.1017/S0373463319000973 Published online by Cambridge University Press

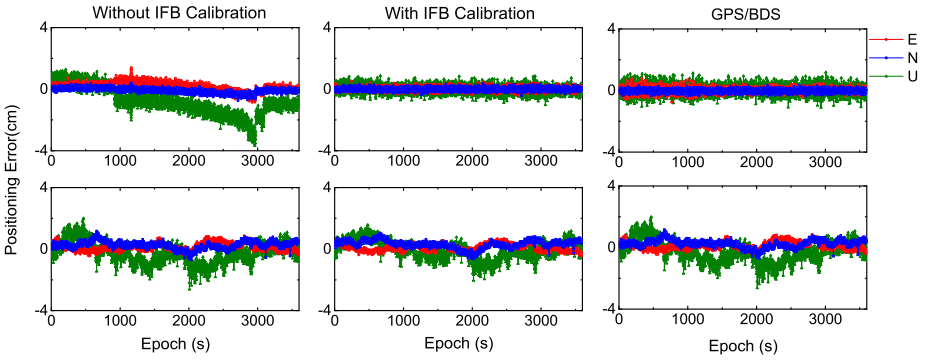

Figure 12. Position errors with IFB calibration compared with no IFB calibration and GPS/BDS for baseline CUT0-CUT1 (top three subgraphs) and baseline HKWS-HKKS (bottom three subgraphs).

because the IFPB rate of baseline CUT0-CUT1 is only a few millimetres, but the positioning results are affected by IFPB rate. GLONASS satellites cannot be positioned normally due to the influence of millimetre-level IFPB rate, which means that positioning results are exactly the same as GPS/BDS. After IFB calibration, the positioning results of baseline CUT0-CUT1 can be significantly improved, and the GLONASS ambiguity of baseline HKWS-HKKS can be substantially fixed. In addition, the GNSS positioning results with IFB calibration are 10%–20% better than GPS/BDS due to the calibrated GLONASS measurements.

Although the constant and real-time IFPB rates estimated by this algorithm exhibit remarkable accuracy and stability, the effects of IFPB rate accuracy on positioning results need to be further analysed to ensure the availability of constant and real-time IFPB rates. The mean values of real-time IFPB rates are used as the accurate IFPB rate, and certain errors (several millimetres) are added on this accurate rate to calculate the positioning results with constant IFPB calibration. Figure 13 shows the influence of IFPB accuracy on the positioning results and ambiguity fixed rates for baselines CUT0-CUT1 and HKWS-HKKS. In Figure 13, when the errors of IFPB rates are within 5 mm, the positioning root mean square (RMS) will slightly decrease as the errors of the IFPB rate increase, but the ambiguity fixed rates are unaffected. When the errors of IFPB rate exceed 5 mm, the ambiguity fixed rates decrease sharply with poor positioning results. Therefore, the accuracy of constant and real-time IFPB rates estimated by this algorithm can meet the requirements of precise positioning.

The positioning results and ambiguity fixed rates for the four types of inhomogeneous baselines are calculated separately to analyse the influence of two IFPB and IFCB calibration methods. Table 3 shows the statistics of position RMS and ambiguity fixed rates with two IFPB and IFCB calibration methods compared with GPS/BDS. Method 1 indicates constant IFPB and IFCB calibration, and Method 2 indicates real-time IFPB and IFCB calibration. In Table 3, with two IFPB and IFCB calibration methods, the position RMS of the multi-GNSS in the horizontal direction are about 1 cm, and the position RMS in the vertical direction are better than 4 cm. Ambiguity fixed rates are also more than 97% for short baseline and more than 88% for medium baseline, which are better than the positioning results of GPS/BDS. The positioning results with real-time IFPB and IFCB calibration are

https://doi.org/10.1017/S0373463319000973 Published online by Cambridge University Press

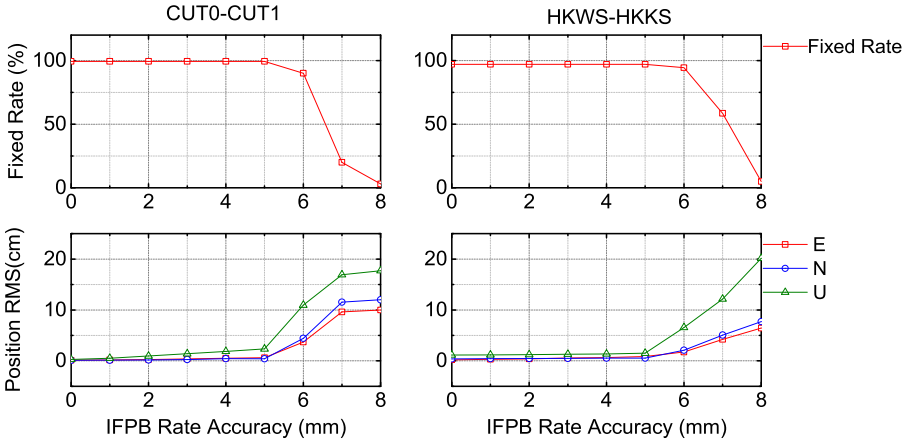

Figure 13. Influence of IFPB accuracy on the positioning results and ambiguity fixed rates for baselines CUT0-CUT1 and HKWS-HKK.

Table 3. Position RMS and ambiguity fixed rate with two IFPB and IFCB calibration methods compared with GPS/BDS.

Baselines	Method	E (cm)	N (cm)	U (cm)	Fixed rate (%)
CUT0-CUT1	Method 1	0·11	0·10	0·27	99·4
	Method 2	0·14	0·12	0·30	99·4
	GPS/BDS	0·16	0·13	0·33	96·5
WUS1-WUU1	Method 1	0·15	0·14	0·88	97·0
	Method 2	0·23	0·20	1·05	97·0
	GPS/BDS	0·27	0·25	1·42	93·8
HKWS-HKKS	Method 1	0·36	0·31	1·14	99·1
	Method 2	0·42	0·36	1·22	99·1
	GPS/BDS	0·51	0·43	1·53	95·7
HKKT-HKKS	Method 1	0·88	0·74	3·02	88·2
	Method 2	1·18	0·99	3·59	88·2
	GPS/BDS	1·40	1·16	3·93	84·2

Note: Method 1: real-time IFPB and IFCB calibration; Method 2: constant IFPB and IFCB calibration.

10%–20% better than those with constant IFPB and IFCB calibration due to the influence of IFPB residual errors, especially on long baselines.

When real-time calibration cannot be implemented under satellite-deprived environments, the enhancements of constant IFB calibrated GLONASS observations for GPS/BDS positioning performance will be verified with different satellite cut-off elevation angles. Figure 14 shows the number of GLONASS satellites with different cut-off elevation angles (from 10° to 40°). Figure 15 shows the position RMS of multi-GNSS and GPS/BDS with different cut-off elevation angles. Figure 16 shows the improvement of multi-GNSS positioning accuracy with IFB calibration compared with GPS/BDS with different satellite cut-off elevation angles. In Figure 14, when cut-off elevation angle is set to less than 20°, the number of GLONASS satellites is from four to six, when cut-off elevation angle is set to more than 20°, the number of GLONASS satellites is two or three. The participation of the GLONASS system can still increase the number of visible satellites as appropriate.

https://doi.org/10.1017/S0373463319000973 Published online by Cambridge University Press

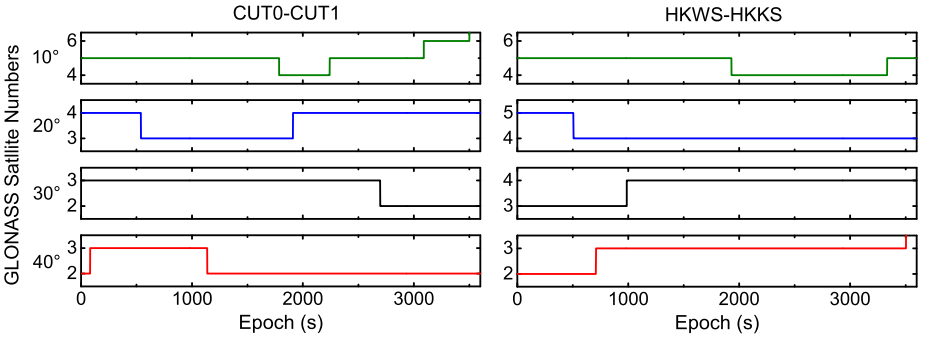

Figure 14. Number of GLONASS satellites with different satellite cut-off elevation angles for baselines CUT0-CUT1 and HKWS-HKKS (from 10° to 40°).

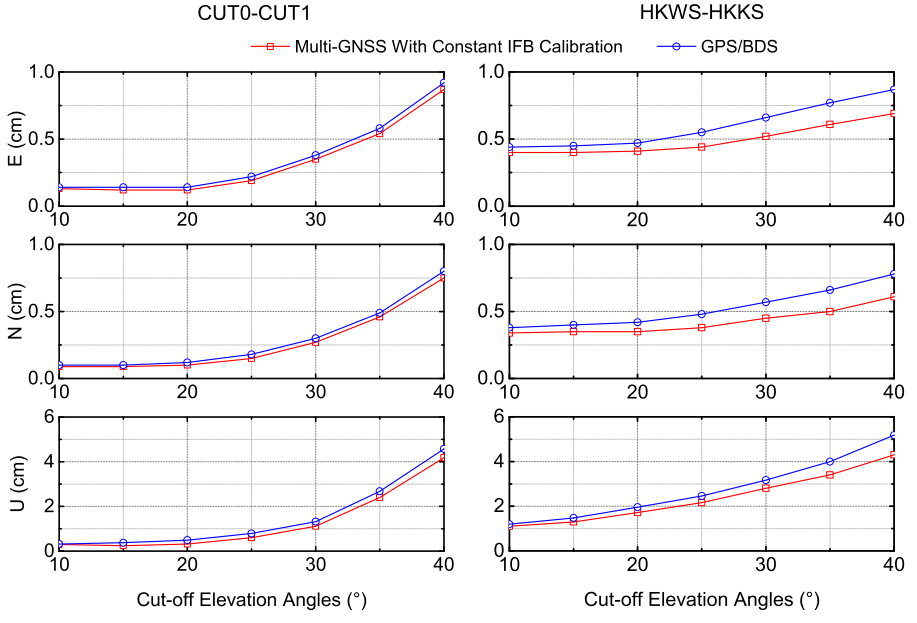

Figure 15. Position RMS of multi-GNSS and GPS/BDS with different cut-off elevation angles for baselines CUT0-CUT1 and HKWS-HKKS.

As shown in Figures 15 and 16, under open-sky environments, the number of GPS/BDS satellites is so large that the multi-GNSS positioning accuracy with GLONASS IFB calibration can be only improved by a few millimetres compared with GPS/BDS when the cut-off elevation angle is set to less than 20°. However, under satellite-deprived environments, for example, an urban canyon with tall buildings, GPS/BDS positioning results are significantly reduced when cut-off elevation angle is increased from 20° to 40°, especially in the vertical direction. When calibrated GLONASS measurements participate in the solution process, the improvement of multi-GNSS positioning accuracy gradually increases as the satellite cut-off elevation angle increases compared with GPS/BDS in Figure 16. This improvement is up to 0·4 cm for zero baseline and 0·9 cm for short baseline in the vertical direction when the cut-off elevation angle rises to 40°.

https://doi.org/10.1017/S0373463319000973 Published online by Cambridge University Press

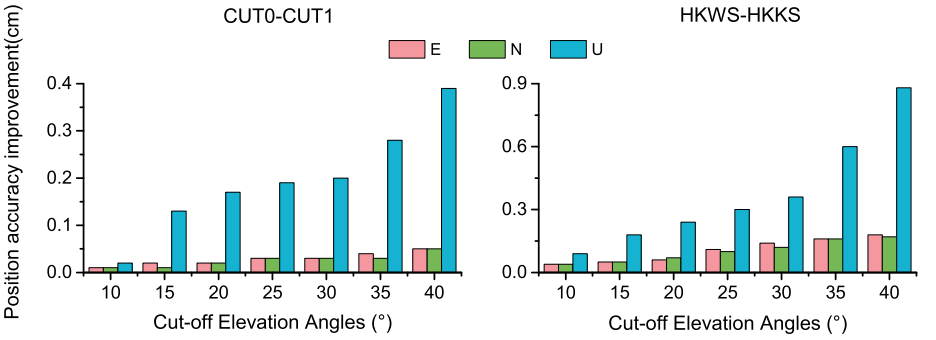

Figure 16. The improvement of multi-GNSS positioning accuracy with IFB calibration compared with GPS/BDS with different satellite cut-off elevation angles for baselines CUT0-CUT1 and HKWS-HKKS.

4. CONCLUSION. Constant IFPB and IFCB may be unavailable or unreliable due to the increasing number of receiver brands from different receiver manufacturers in recent years. Both IFPB and IFCB are susceptible to receiver firmware version, antenna type, environment and other factors. In this study, a fast, real-time, accurate and reliable estimation and calibration algorithm for IFPB and IFCB without initial values is proposed based on multi-GNSS assistance. In this algorithm, real-time IFPB rate and IFCB will be estimated and calibrated based on multi-GNSS assistance by providing fixed solution coordinates, and IFPB calibration can be divided into constant and real-time IFPB calibration to meet different requirements.

Several experiments were conducted to validate the performance of this algorithm. First, constant IFPB rate, real-time IFPB rate and IFCB were estimated. The results show that constant IFPB rate, obtained within several seconds for short baseline and several minutes for medium baseline, has only a 2 mm difference from the mean value of real-time IFPB rate. Moreover, the real-time IFPB rate has remarkable stability with STD less than 0·25 mm. The IFCB STD is also within 0·2 m, and the change in reference satellite cannot affect the results of IFPB rate and the stability of IFCB. Second, several positioning performances are analysed, and the results show that the ambiguity fixed rates are unaffected when the errors of the IFPB rate are within 5 mm, whereas the positioning RMS will decrease slightly as the errors of the IFPB rate increase. Centimetre-level positioning results can be obtained with IFPB and IFCB calibration, and their GLONASS ambiguity fixed rate is higher than 97% and 88% for short and medium baselines, respectively. The positioning results with constant IFPB calibration are 10%–20% worse than real-time IFPB rate calibration. Under satellite-deprived environments, such as urban canyons, the improvements of multi-GNSS positioning accuracy with constant IFB calibration gradually increase as the satellite cut-off elevation angle increases compared with GPS/BDS, which can reach up to 0·9 cm in the vertical direction when the cut-off elevation angle rises to 40°.

ACKNOWLEDGEMENTS

This work is funded by the National Key Research and Development Program of China (No. 2016YFB0800405). In addition, it is part of the project 'Research on Real-time and High-accuracy Multi-GNSS Location Based Service Platform' (No. 2018010401011271), which is supported by the Wuhan Science and Technology Bureau. Moreover, the authors are grateful to Curtin

GNSS Research Centre and Hong Kong Satellite Positioning Reference Station Network for multi-GNSS data in this study. All this support is gratefully acknowledged. The authors are grateful to anonymous reviewers for their insightful comments, which have helped to improve the quality of the study.

REFERENCES

Al-Shaery, A., Zhang, S. and Rizos, C. (2013). An enhanced calibration method of GLONASS inter-channel bias for GNSS RTK. *GPS Solutions*, 17(2), 165–173.

Banville, S., Collins, P. and Lahaye, F. (2013). GLONASS ambiguity resolution of mixed receiver types without external calibration. *GPS Solutions*, 17(3), 275–282.

Jiang, W.P., An, X.D., Chen, H. and Zhao, W. (2017). A new method for GLONASS inter-frequency bias estimation based on long baselines. *GPS Solutions*, 21(4), 1765–1779.

Karutin, S. and Inst, N. (2015). GLONASS Program Update. *Proceedings of the 28th International Technical Meeting of the Satellite Division of the Institute of Navigation*, Tampa, FL, 1207–1221.

Liu, Y.H., Li, X.H., Zhang, H.J., Zhu, F. and Ren, Y. (2016). Calculation and accuracy evaluation of TGD from IFB for BDS. *GPS Solutions*, 20(3), 461–471.

Liu, Y.Y., Gu, S.F. and Li, Q.Q. (2018). Calibration of GLONASS inter-frequency code bias for PPP ambiguity resolution with heterogeneous rover receivers. *Remote Sensing*, 10(3), 19.

Pratt, M., Burke, B. and Misra, P. (1998). Single-epoch integer ambiguity resolution with GPS-GLONASS L1-L2 data. *Proceedings of Ion Gps*, Cambridge, MA, 11, 691–699.

Reussner, N. and Wanninger, L. (2011). GLONASS Inter-frequency Biases and Their Effects on RTK and PPP Carrier-phase Ambiguity Resolution. *Proceedings of the 24th International Technical Meeting of the Satellite Division of the Institute of Navigation*, Portland, OR, 712–716.

Revnivykh, S. (2011). GLONASS Status and Modernization. *Proceedings of the 24th International Technical Meeting of the Satellite Division of the Institute of Navigation*, Portland, OR, 839–854.

Shi, C., Yi, W.T., Song, W.W., Lou, Y.D., Yao, Y.B. and Zhang, R. (2013). GLONASS pseudorange inter-channel biases and their effects on combined GPS/GLONASS precise point positioning. *GPS Solutions*, 17(4), 439–451.

Song, W.W., Yi, W.T., Lou, Y.D., Shi, C., Yao, Y.B., Liu, Y.Y., Mao, Y. and Xiang, Y. (2014). Impact of GLONASS pseudorange inter-channel biases on satellite clock corrections. *GPS Solutions*, 18(3), 323–333.

Takac, F. (2009). GLONASS inter-frequency biases and ambiguity resolution. *Inside GNSS*, 4(2), 24–28.

Tian, Y., Ge, M. and Neitzel, F. (2015). Particle filter-based estimation of inter-frequency phase bias for real-time GLONASS integer ambiguity resolution. *Journal of Geodesy*, 89(11), 1145–1158.

Tian, Y., Ge, M., Neitzel, F., Yuan, L., Huang, D., Zhou, L. and Yan, H. (2018). Improvements on the particle-filter-based GLONASS phase inter-frequency bias estimation approach. *GPS Solutions*, 22(3), 71.

Wang, J. (2000). An approach to GLONASS ambiguity resolution. *Journal of Geodesy*, 74(5), 421–430.

Wanninger, L. (2012). Carrier-phase inter-frequency biases of GLONASS receivers. *Journal of Geodesy*, 86(2), 139–148.

Wanninger, L. and Wallstab-Freitag, S. (2007). Combined Processing of GPS, GLONASS, and SBAS Code Phase and Carrier Phase Measurements. *Proceedings of the 20th International Technical Meeting of the Satellite Division of the Institute of Navigation*, Fort Worth, TX, 866–875.

Yamada, H., Takasu, T., Kubo, N. and Yasuda, A. (2010). Evaluation and Calibration of Receiver Inter-channel Biases for RTK-GPS/GLONASS. *Proceedings of the 23rd International Technical Meeting of the Satellite Division of the Institute of Navigation*, Portland, OR, 1580–1587.

Yao, Y.B., Hu, M.X., Xu, X.Y. and He, Y.D. (2017). GLONASS inter-frequency phase bias rate estimation by single-epoch or Kalman filter algorithm. *GPS Solutions*, 21(4), 1871–1882.